150 (2026) 205900

Contents lists available at ScienceDirect

Gas Science and Engineering

journal homepage: www.journals.elsevier.com/gas-science-and-engineering

Low-energy CO_2 capture via guanidinium sulfate clathrate from flue gas

Chongwei Wang [a], Shuanshi Fan [a,b,*], Yanhong Wang [a], Xuemei Lang [a,b], Siyuan Chen [a], Gang Li [a]

[a] School of Chemistry and Chemical Engineering, South China University of Technology, Guangzhou, 510640, China
[b] Key Laboratory of Heat and Mass Transfer and Low-Carbon Conversion, Ministry of Education, South China University of Technology, Guangzhou, 510640, China

ARTICLE INFO

Keywords:
Clathrate
Flue gas
Gua_2SO_4
CO_2 capture
Energy consumption

ABSTRACT

Clathrate technology, as an effective approach, is widely applied in fields such as carbon capture and gas storage. However, low gas selectivity and high energy consumption limit its development. Therefore, an innovative gas separation technology based on guanidinium sulfate (Gua_2SO_4) clathrate is proposed for efficient CO_2 capture. This study investigated the phase equilibrium conditions of 14.8 mol% CO_2/85.2 mol% N_2 + Gua_2SO_4 system at temperature ranging from 283.6 K to 291.1 K and pressure from 2.0 MPa to 3.3 MPa. The results indicated that Gua_2SO_4 could effectively lower the formation conditions of the clathrate. Based on phase equilibrium conditions, the separation of flue gas using Gua_2SO_4 was further investigated. At 280.6 K and 3.0 MPa, the CO_2 in the clathrate phase reached 81.4 mol% with the CO_2 capture rate 63.1 %. This demonstrated the potential of Gua_2SO_4 in carbon capture technology for treating flue gas. Additionally, after treatment with a Gua_2SO_4 solution, the N_2 concentration in the gas phase increased significantly with a separation factor of 55.0, which demonstrated the high selectivity and potential of Gua_2SO_4 in carbon capture technology. Using Aspen HYSYS, an energy consumption analysis for CO_2 capture was conducted at 3.0 MPa and 2.0 MPa with conditions of 280.6 K. Calculations revealed that the lowest energy consumption for CO_2 capture was 0.69 kWh/kg and 0.56 kWh/kg CO_2. Compared to current literature, this lower energy consumption is significant for subsequent gas separation and carbon capture processes.

1. Introduction

Massive CO_2 emissions led to global temperature increases, triggering extreme weather events, including droughts, floods, and hurricanes. This leads to consequences such as glacial melting and sea level rise, which disrupt the balance of ecosystems (Davoodi et al., 2023). Coal-fired power plants continue to be a major source of electricity generation worldwide. The primary components of flue gas from coal-fired power plants are N_2 and CO_2, with the volume fraction of CO_2 typically ranging between 15 % and 30 %. Therefore, the capture of CO_2 from flue gas streams has become an essential strategy for mitigating climate impact. Currently prevalent CO_2 capture techniques include chemical absorption (Aghel et al., 2022), pressure swing adsorption (Lin et al., 2017), temperature swing adsorption (Wu et al., 2025), membrane separation (Ye et al., 2024; Chen et al., 2025; Li et al., 2023; Gao et al., 2025), cryogenic separation (Fu et al., 2022), Ionic liquid adsorption (Li et al., 2026a; Wang et al., 2026; Xia et al., 2026), and hydrate-based gas separation (Huang et al., 2022; Fan et al., 2016). Absorption-based capture technologies are mature but suffer from high regeneration energy demand as well as solvent degradation and corrosion issues. Adsorption and membrane processes require less thermal energy; however, their performance is sensitive to feed fluctuations and impurities and often necessitates multistage separation to achieve high purity. Ionic liquids suffer from stability issues, particularly evaporation losses, which hinder their large-scale deployment. Cryogenic separation can achieve high-purity CO_2, but it is typically energy-intensive when applied to dilute post-combustion gas streams. By contrast, hydrate-based separation exploits the inherent thermodynamic selectivity between CO_2 and N_2. When combined with suitable promoters, this approach enables simultaneous CO_2 enrichment and nitrogen recovery while exhibiting relatively low sensitivity to operating conditions. Among these technologies, hydrate-based gas separation demonstrates significant advantages due to their unique thermodynamic selectivity and environmentally friendly characteristics. The separation mechanism stems from the differing phase equilibrium conditions required for CO_2 and N_2 to form hydrates. At 273.0 K, the phase

* Corresponding author. School of Chemistry and Chemical Engineering, South China University of Technology, Guangzhou, 510640, China.
E-mail address: ssfan@scut.edu.cn (S. Fan).

https://doi.org/10.1016/j.jgsce.2026.205900
Received 30 October 2025; Received in revised form 26 January 2026; Accepted 10 March 2026
Available online 11 March 2026

equilibrium pressure for CO_2 hydrates was 1.2 MPa (Ito et al., 2023), whereas N_2 hydrates required pressures as high as 15.0 MPa to remain stable (Mohammadi and Richon, 2010). This significant pressure difference enabled selective CO_2 capture under moderate pressure conditions (1.0-5.0 MPa). Experimental studies indicated that, under optimized conditions (277.7 K, 2.2 MPa), this technology achieved a separation factor exceeding 30 for CO_2/N_2 mixture (Fan et al., 2009). Compared to conventional carbon capture technologies, the hydrate method offers significant advantages: (1) Its selective separation mechanism, based on thermodynamic differences at the molecular scale, exhibits strong adaptability to fluctuations in flue gas flow; (2) Using water as the primary reaction medium avoids the environmental risks associated with organic solvents; (3) Optimizing the additive system can effectively reduce reaction pressure and increase operating temperature, thereby further lowering energy consumption. However, practical application of hydrate-based CO_2 capture has been hindered by unfavorable formation conditions, slow kinetics, and relatively high energy consumption associated with gas compression and refrigeration.

To address these challenges, various thermodynamic promoters have been introduced to shift hydrate equilibrium toward higher temperatures and lower pressures. Kim et al. (Bai et al., 2025) examined the influence of cyclopentane (CP) on hydrate formation from a simulated flue gas mixture (CO_2/N_2). Their results demonstrated that the addition of CP significantly moderates the phase equilibrium conditions relative to pure water, notably increasing the equilibrium temperature by approximately 19 K at 10.0 MPa, the CO_2 concentration in the hydrate phase attained 61.0 mol%. Yang et al. (2018) investigated hydrate formation when CO_2/N_2 gas mixture and water interacted in the presence of THF. The addition of THF improved the original phase equilibrium conditions for hydrate formation and significantly shortened the induction time of the process. Fan et al. (2009) studied the kinetics of hydrate formation using simulated power plant flue gas in systems containing TBAB and 0.293 mol% TBAF. The presence of these additives markedly shifted the hydrate phase equilibrium boundary toward higher temperatures and lower pressures. As the TBAB concentration increased, the driving force for the reaction between water and the reactants grew stronger, accelerating the reaction rate. Under conditions of 277.7 K and 2.19 MPa in the presence of TBAF, 90.4 mol% CO_2 and 50 % capture rate were achieved. Xu et al. (2025) studied hydrate formation using simulated flue gas (20 mol % CO_2/80 mol% N_2) with TBAF thermodynamic promoter. As the TBAF concentration increased from 5 wt% to 20 wt%, the phase equilibrium conditions between CO_2 and N_2 became more favorable. Compared to pure water systems, the CO_2/N_2 hydrate exhibited a reduced induction time, an increased formation rate, and a higher gas absorption capacity. In the presence of TBAF, the formation pressure for the clathrate compound decreased; however, other gases in the mixture became trapped within the clathrate cage, resulting in low capture efficiency. Li et al. (2012) compared the separation performance of TBAB, $TBANO_3$, and TBPB for mixture containing 17 mol% CO_2. They found induction times of less than 5 min across all systems. Among these, $TBANO_3$ demonstrated the most outstanding performance, exhibiting the highest gas consumption, a CO_2 capture rate of 67 %, and a separation factor of 15.54-1.5 times that of the TBAB system—revealing excellent kinetic characteristics. Common additives promote the encapsulation of guest molecules by either forming their own dominant hydrates or participating in the formation of hydrate cages (Lv et al., 2023; Sun et al., 2011; Chen et al., 2023a, 2024). Research indicates that enhancing reaction driving force can effectively improve reaction efficiency, while constructing highly selective reaction systems is key to achieving efficient separation (Seo et al., 2023a, 2023b). Notably, some accelerators used in early studies exhibited issues such as volatility, toxicity, and environmental pollution (Xia et al., 2022). In recent years, research trends have shifted toward developing novel low-toxicity, and environmentally friendly promoters (Zhang et al., 2020). Consequently, creating new chemical promoters that combine high efficiency, environmental sustainability, and recyclability has become a primary focus in hydrate-based CO_2 capture technology research.

Carbon capture technologies have been demonstrated to be technically feasible, and the focus of current research should therefore shift toward the evaluation of energy consumption. Zheng et al. proposed a two-stage hydrate-based capture system integrated with energy recovery techniques. By optimizing operating conditions, the system achieved reduced energy consumption while maintaining a CO_2 purity exceeding 95 mol% (Zheng et al., 2024). Li et al. developed a novel integrated system combining compressed air energy storage with carbon capture to enhance the operational flexibility of coal-fired power plants and reduce CO_2 emissions. Through system optimization, improved energy efficiency was demonstrated (Li et al., 2026b). Eder explored a novel hydrate-based CO_2 capture process and demonstrated significantly enhanced formation kinetics and improved CO_2 selectivity at low temperature (233 K) and moderate pressure (40 bar). Under continuous operation, the system achieved a CO_2 capture rate of 0.295 g $L^{-1}\cdot min^{-1}$ with a specific energy consumption lower than 0.83 kWh/kg CO_2 captured, indicating its competitiveness relative to conventional carbon capture technologies (Eder et al., 2025). Compared with time-consuming and cost-intensive experimental studies, process simulation represents a promising alternative approach for evaluating and optimizing carbon capture processes prior to the construction of physical pilot plants. The primary objective of this study is to assess the energy efficiency and feasibility of a novel Gua_2SO_4-promoted clathrate-based CO_2 capture process by integrating experimental performance with process simulation, thereby evaluating its potential for large-scale application.

Recent study has identified Gua_2SO_4 as a promoter capable of forming clathrate-like complexes with CO_2 under moderate temperature and pressure. The structure of Gua_2SO_4 favors selective CO_2 uptake over other gases, such as N_2 or H_2, due to specific electrostatic interactions between the guanidinium ions and CO_2 (Xiang et al., 2023). Unlike typical physisorption or chemisorption processes, where other gases often interfere with the capture process, Gua_2SO_4 selectively captures CO_2, even in the presence of H_2. This high selectivity arises from the unique interaction between CO_2 and the Gua_2SO_4 structure, which prevents the capture of other gases via the same electrostatic interactions. Due to the high water solubility of Gua_2SO_4, CO_2 introduced into water was rapidly captured by Gua_2SO_4 (Xiang et al., 2023). Gua_2SO_4 exhibits unique advantages as an additive for CO_2 capture. Consequently, Wang et al. (2025) conducted CO_2 complexation experiments using Gua_2SO_4 solutions, confirming the formation of stable CO_2–Gua_2SO_4 cage-like complexes. The application of Gua_2SO_4 presents a promising alternative for CO_2 capture and separation. This work investigates the phase equilibrium conditions of clathrates formed from a flue gas in Gua_2SO_4 solution, as well as the kinetics of CO_2 sequestration across varying driving forces. To improve both the efficiency of CO_2 capture and the resulting gas purity, this study examined how varying driving forces and Gas-liquid ratio (R_v) influence the separation of flue gas mixture. Additionally, using Aspen HYSYS, an energy consumption analysis for CO_2 capture was conducted. Energy consumption is a critical indicator for evaluating the industrial feasibility of CO_2 capture technologies. However, most studies on clathrate-based separation technologies have primarily focused on phase equilibrium and separation performance, while comparatively less attention has been paid to energy analysis and process integration. Therefore, it is necessary to conduct a comprehensive energy assessment that links experimental separation performance with process simulation, energy recovery, and operating conditions, to better understand the practical potential of clathrate-based CO_2 capture systems. Through such combined experimental and energy-consumption analysis, this study aims to elucidate the potential advantages and limitations of the Gua_2SO_4–promoted clathrate technology and to provide a more comprehensive basis for evaluating its applicability in post-combustion CO_2 capture.

2. Experimental materials and methods

2.1. Experimental materials

Simulated flue gas (14.8 mol% CO_2-85.2 mol% N_2) was supplied by Foshan Kedi Gas Chemical Co., Ltd. 99.0 wt% Gua_2SO_4 was provided by Shanghai MacLean Biochemical Technology Co., Ltd. Deionized water was prepared in our laboratory. All chemicals were used as received without additional treatment.

2.2. Experimental equipment

The phase equilibrium apparatus applied in the current investigation has been described in detail in our previous work (Fan et al., 2019; Qi et al., 2018; Chen et al., 2023b).

Fig. 1 provides a schematic overview of the experimental system. The core component was a high-pressure clathrate reactor, designed for pressures up to 20.0 MPa. The reactor is equipped with an internal mechanical stirrer. It has a volume of 250 ml, and an internal diameter of 50 mm. Temperature was monitored using a PT-100 probe (accuracy: ±0.1 K; Shanghai Yijia Electric Heating Co., Ltd.), while pressure was measured with a transducer (accuracy: ±0.04 MPa; Guangzhou Senex Instrument Co., Ltd.). A data acquisition system, linked to a remote monitor, recorded all measurements. Evacuation was performed using a vacuum pump (model: 2XZ-4; Linhai Yonghao Vacuum Equipment Co., Ltd.) with a rotational speed of 1400 r/min and a pumping capacity of 4 L/s. Temperature control was maintained by a refrigeration circulator (model: F-32; JULABAO Technologies, Ltd.) accurate to ±0.1 K. Gas composition was analyzed using a GC9800 gas chromatograph (Shanghai Kechuang Chromatography Instrument Co., Ltd.), which was fitted with a thermal conductivity detector and a TDX-01 column.

2.3. Experimental procedure

Building on previous studies which demonstrated the superior CO_2 capture capacity of aqueous Gua_2SO_4 at 72.0 wt% concentration (Wang et al., 2025), the present work adopted this specific concentration for further investigation. A series of experiments were conducted to assess the effects of critical operating variables—such as temperature and pressure on the performance of CO_2 capture and separation. Before conducting the test, the integrity of the reactor was verified by pressurizing the system with N_2 to 8.0 MPa and confirming that pressure remained stable (±0.02 MPa) for 2 h under isothermal conditions. Temperature control was achieved using a water bath. Following thermal stabilization at the desired value, the reactor was repeatedly flushed with a simulated flue gas to eliminate any residual air. A predetermined volume of Gua_2SO_4 solution was then introduced into the evacuated reactor. After the temperature was stabilized, the gas mixture was charged to the target pressure, and mixing was initiated via mechanical agitation. Clathrate formation was identified by a consistent drop in system pressure. The reaction was considered complete once the pressure stabilized, defined as a variation of less than 0.02 MPa over 1 h. Finally, the composition of the equilibrium gas phase was quantified using gas chromatography.

2.4. Analysis methods

2.4.1. Gas consumption

Gas consumption, denoted as Δn, refers to the molar quantity of gas absorbed during clathrate formation and is computed using equations (1) and (2).

$$PV = ZnRT \tag{1}$$

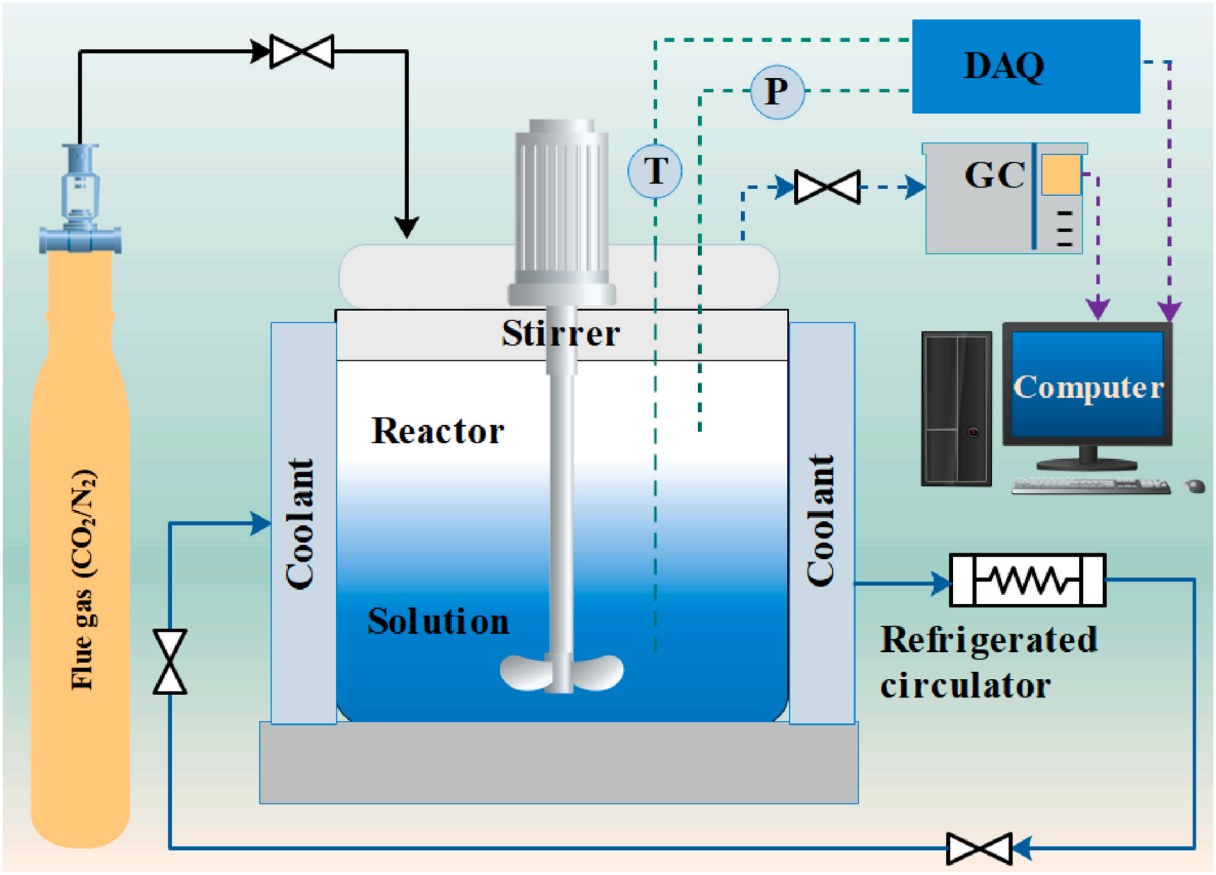

Fig. 1. The schematic diagram of the experimental apparatus for CO_2 capture by Gua_2SO_4 clathrate.

$$\Delta n = n_0 - n_t = P_0 V_0 / Z_0 R T_0 - P_t V_t / Z_t R T_t \quad (2)$$

The total moles of gas consumed, denoted as Δn, are determined based on the reactor temperature (T), pressure (P), the universal gas constant (R), and the compression factor (Z) derived from the Peng–Robinson equation (Peng and Robinson, 1976). The subscripts 0 and t correspond to the initial condition and time t, respectively, while V represents the gas-phase volume.

It should be noted that the gas uptake calculated from the pressure drop represents an apparent uptake, assuming perfect system sealing and that gas consumption is dominated by clathrate formation. In highly concentrated Gua_2SO_4 solutions, a fraction of CO_2 may also dissolve into the liquid phase due to gas–liquid equilibrium effects. Although the presence of a concentrated electrolyte is expected to significantly reduce CO_2 solubility through salting-out effects, this contribution is not explicitly separated from clathrate uptake in the present analysis. Therefore, the reported gas uptake values should be interpreted as an upper-bound estimate of clathrate-associated gas consumption under the investigated conditions.

2.4.2. CO_2 capture rate

The CO_2 capture rate is defined as the amount of CO_2 in the clathrate divided by the amount of raw gas CO_2 and is expressed as R_{CO_2}, It can be calculated using the following equation 3

The CO_2 capture rate denoted as R_{CO_2} is defined as the rate of CO_2 trapped within the clathrate phase to the original CO_2 present in the feed gas. It is calculated as follows (Di Profio et al., 2017):

$$R_{CO_2} = n^C_{CO_2} \Big/ n^0_{CO_2} \times 100\ \% \quad (3)$$

In equation (3), $n^C_{CO_2}$ denotes the amount of CO_2 in the clathrate mixture, $n^0_{CO_2}$ denotes the initial amount of CO_2 in the mixture used.

2.4.3. Separation factor (SF)

The CO_2 separation factor is defined as the ratio of (CO_2/N_2) in the clathrate phase to in the gas phase (Li et al., 2016), as calculated by equation (4).

$$SF = \frac{n^C_{CO_2}}{n^C_{N_2}} \Big/ \frac{n^G_{CO_2}}{n^G_{N_2}} \quad (4)$$

$n^G_{CO_2}$ denotes the amount of N_2 in the gas phase mixture, $n^C_{N_2}$ denotes the amount of N_2 in the clathrate phase mixture, $n^G_{N_2}$ denotes the amount of N_2 in the gas phase mixture.

2.4.4. Gas-liquid ratio (G/L)

(G/L) is calculated by equation (5).

$$R_v = G/L = V^G_0 / V^L_t = 22400 n_0 / V^L_t \quad (5)$$

At standard temperature and pressure, 22400 mL/mol is the volume occupied by a gas per unit amount of substance. V^G_0 denotes the volume of the gas phase at initial time, n is the number of moles of gas, subscript 0 denotes the initial time, V^L_t denotes the volume of the liquid phase at time t (Wang et al., 2026).

2.4.5. Residual gas-phase CO_2 concentration

The residual gas-phase concentration of CO_2 was measured by gas chromatography.

2.4.6. Clathrate phase CO_2 concentration (CP_{CO2})

The HP_{CO2} is expressed as described by equation (6),

$$CP_{CO_2} = n^C_{CO_2} \Big/ \left(n^C_{CO_2} + n^C_{CO_2} \right) \times 100\ \% \quad (6)$$

In this study, the separation factor (SF) is used to indicate the relative ease of CO_2/N_2 separation. As defined in equation (4), SF compares the CO_2/N_2 ratio in the clathrate phase with that in the gas phase and thus reflects intrinsic selectivity. However, SF alone does not determine process performance, which also depends on the extent of CO_2 capture and the absolute phase compositions. Therefore, SF should be interpreted together with the CO_2 concentration in the clathrate phase, the N_2 purity in the residual gas, and the CO_2 capture rate. Under the investigated conditions, higher SF values correspond to stronger CO_2 enrichment in the clathrate phase and higher N_2 fractions in the residual gas. From a process perspective, CO_2 product purity and recovery are the key performance indicators; accordingly, SF is considered a complementary selectivity descriptor rather than a standalone metric.

3. Results and discussion

3.1. Clathrate phase equilibrium

The phase equilibrium conditions of flue gas with 72.0 wt% Gua_2SO_4 solution were measured across temperatures from 283.6 K to 291.1 K and pressures between 2.0 MPa and 3.3 MPa. Fig. 2 shows the clathrate equilibrium curves of CO_2+H_2O (Fan and Guo, 1999), N_2+ H_2O (Mohammadi and Richon, 2010), CO_2+H_2O+(33.1 wt%)TBAF (Lee et al., 2012), N_2+ H_2O+(34.0 wt%)TBAF (Lee et al., 2010), CO_2+(40 wt %)TBAB (Lee et al., 2011), N_2+(40 wt%)TBAB (Lee et al., 2010), CO_2+72.0 wt% Gua_2SO_4 solution (Wang et al., 2025; Fan et al., 2016) 0.8 mol% CO_2-85.2 mol% N_2 +72.0 wt% Gua_2SO_4 systems. TBAB and TBAF, as organic salt additive, represent current promotor with favorable thermodynamic promotion effects. Based on phase equilibrium principles, the addition of TBAB promotes the formation of clathrate complexes with CO_2 and N_2 under conditions of elevated temperature and reduced pressure. Fig. 2 displays the phase equilibrium behavior of the CO_2 + 72.0 wt% Gua_2SO_4 system, indicating that Gua_2SO_4 at this concentration substantially decreases the equilibrium pressure and temperature compared to TBAB and TBAF, demonstrating its enhanced thermodynamic stability and high selectivity in gas separation. Consequently, Gua_2SO_4 was more conducive to CO_2 clathrate complex formation and selective CO_2 capture.

3.2. Pressure and temperature on separation performance

The separation experiment of flue gas using a 72.0 wt % Gua_2SO_4 solution was investigated by varying temperature, pressure and R_v.

3.2.1. Pressure driving force on separation performance

According to the theory proposed by Englezos et al. (1987). The driving force for clathrate reactions stems from the difference between the fugacity of substances in the reaction process and their equilibrium fugacity. The kinetics of clathrate formation can be qualitatively inferred from the pressure–time profiles. Under all investigated conditions, pressure reduction began immediately after reaching the target conditions, indicating the absence of a pronounced induction period and suggesting that Gua_2SO_4 effectively promotes nucleation. Comparisons of the initial pressure-drop rates and overall formation times further show that higher pressure and lower temperature accelerate clathrate formation, providing a semi-quantitative basis for assessing relative kinetics across operating conditions. Table S1 provides the detailed data. As shown in Fig. 3(a), pressure reductions of 0.17 MPa, 0.26 MPa, and 0.3 MPa were observed at initial pressures of 2.0 MPa, 3.0 MPa, and 5.0 MPa, respectively. In experiments, the disparity between actual pressure and equilibrium pressure reflected this fugacity difference. Consequently, higher pressures showed a stronger driving force for the reaction, increasing the formation of clathrates. In our previous study, Raman spectroscopy directly confirmed the formation of Gua_2SO_4-CO_2 clathrates, as evidenced by the characteristic Raman peaks associated with CO_2 molecules trapped within the clathrate cages. This Raman-based confirmation has been widely validated in similar systems,

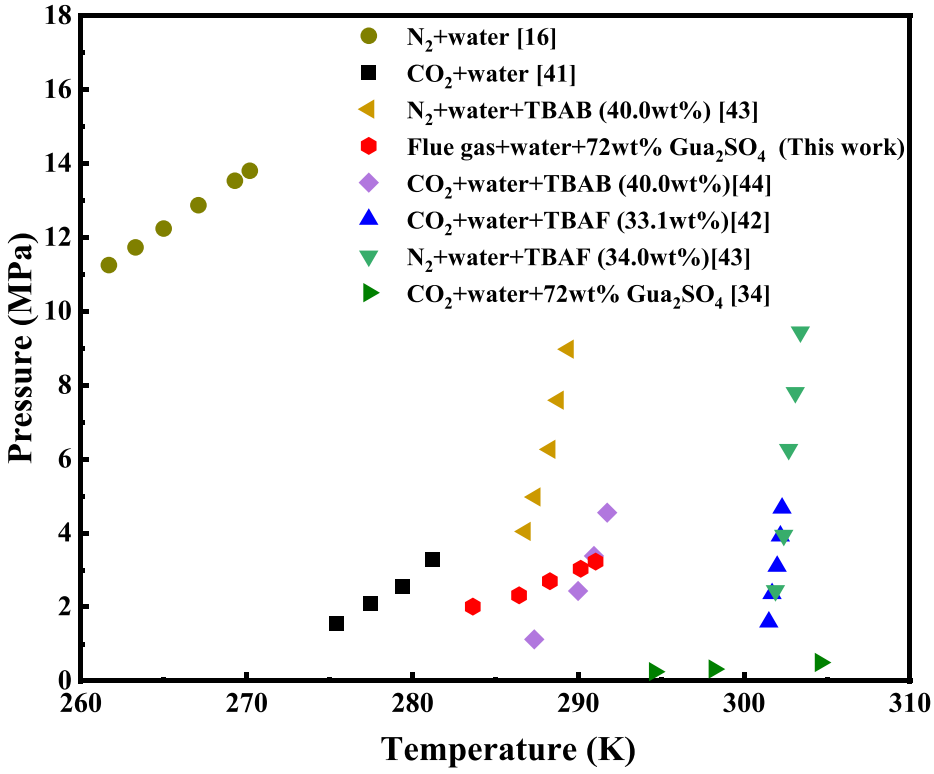

Fig. 2. Clathrate phase equilibrium data for CO_2+water and CO_2, N_2, flue gas in solution, olive ● ref (Mohammadi and Richon, 2010); black■ ref (Fan and Guo, 1999); orange◀ ref (Lee et al., 2010); red● this work; purple◆ ref (Lee et al., 2011); blue▲ ref (Lee et al., 2012); green ▼ ref (Lee et al., 2010); green ▶ ref (Wang et al., 2025). (For interpretation of the references to colour in this figure legend, the reader is referred to the Web version of this article.)

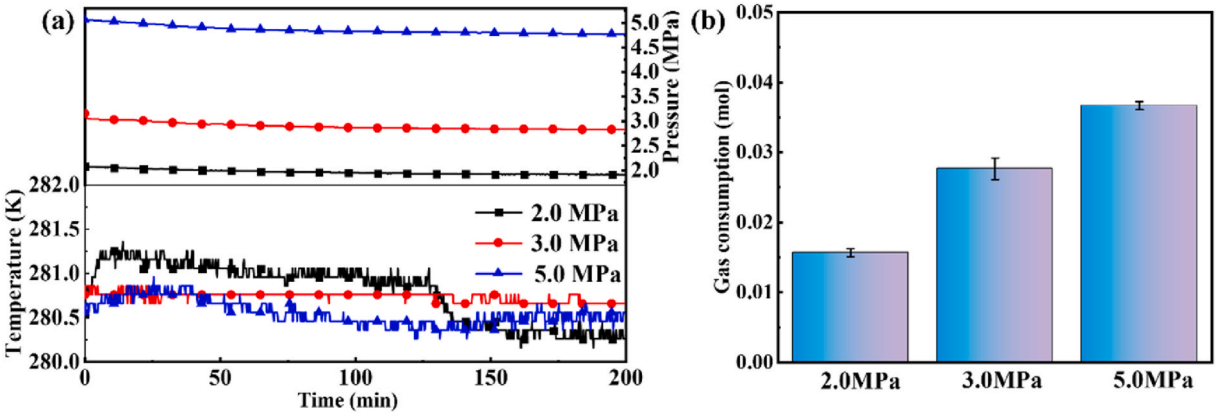

Fig. 3. (a) Pressure changes during clathrate formation and (b) gas consumption at different pressures, a temperature of 280.6 K, and in 72.0 wt % Gua_2SO_4 solution.

as demonstrated in the study by Wang et al., where CO_2 clathrates were synthesized and characterized using Raman spectroscopy (Wang et al., 2025). Additionally, in other study, the structure of Gua_2SO_4-CO_2 clathrates has been confirmed through X-ray diffraction, as reported by Xiang et al., who confirmed the formation of CO_2 clathrates under specific conditions using X-ray diffraction analysis (Xiang et al., 2023).

According to RK equation calculations, when the feed pressure increased from 2.0 MPa to 5.0 MPa, the molar quantity of feed gas raised from 0.18 mol to 0.34 mol. As shown in Fig. 3(b), the molar quantity of gas forming clathrates also increased from 0.017 mol to 0.037 mol. This indicated that higher feed pressures enhance the driving force for clathrate formation, making the gas-to-clathrate conversion trend more pronounced. As shown in Fig. 4(a), the separation factor gradually decreased with increasing pressure. This reduction occurred because elevated pressure allows N_2 gas to enter the liquid phase, thereby diminishing the separation factor. The CO_2 capture rate initially increased from 51.5 % to 63.1 % with rising feed pressure before decreasing to 57.4 %. From 2.0 MPa to 3.0 MPa, the increased pressure enhanced the driving force, leading to higher CO_2 capture. However, from 3.0 MPa to 5.0 MPa, excessively high pressure increased the gas volume, causing N_2 to enter the clathrate phase and resulting in a decrease in R_{CO2}. As illustrated in Fig. 4(b), after clathrate equilibrium was attained, a rise in feed pressure resulted in a decrease of CO_2 concentration in the gas phase from 7.9 mol % to 6.2 mol % and 7 mol %, while CO_2 concentration in the clathrate phase decreased from 83.9 mol % to 76.7 mol %. Under high-pressure conditions, the clathrate

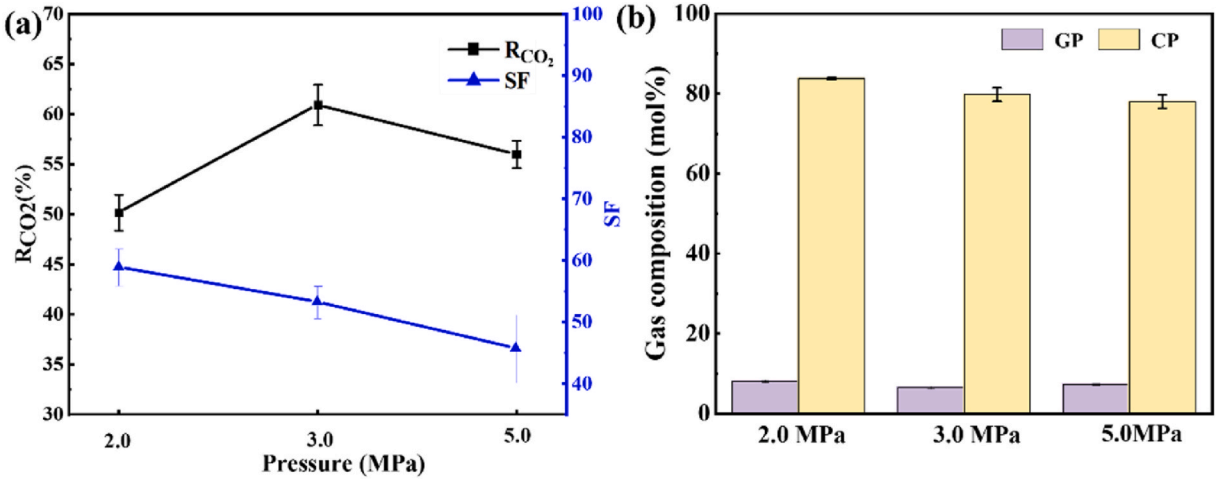

Fig. 4. (a) CO_2 capture rate and separation factor, (b) the CO_2 concentration in the gas phase and clathrate phase at different pressures, a temperature of 280.6 K, and in 72.0 wt % Gua_2SO_4 solution.

compound exhibits a strong affinity for CO_2, enabling more efficient capture from the mixed gas stream and achieving a higher R_{CO2} value. However, as pressure increased, N_2 also became more readily incorporated into the clathrate compound, reducing its selectivity for CO_2. The corresponding decrease in residual gas phase concentration corroborates this.

3.2.2. *Temperature on separation performance*

Table S2 presents a summary of the experimental results obtained under different temperature conditions. As the system temperature decreased from 288.8 K to 280.6 K, the initial reaction slopes of the three curves in Fig. 5(a) increased successively, indicating that the reaction rate increased and the reaction time gradually shorted. This occurs because the decrease in temperature increased the driving force for the formation of gas clathrate complexes at the same supply pressure, thereby promoting the clathrate reaction and reducing the reaction time. As the reaction progressed, the slopes of all three curves in Fig. 5 (a) gradually flattened. Upon reaching equilibrium in the clathrate reaction, the system's equilibrium pressure decreased with lower temperatures, pressure differences of 0.26 MPa, 0.23 MPa, and 0.19 MPa at 280.6 K, 283.2 K, and 288.6 K, respectively. Lower temperatures facilitated the easier formation of gas clathrates.

Fig. 5(b) showed that at 3 MPa, as the initial temperature increased from 280.6 K to 288.8 K, the amount of clathrate compound formed decreased, and the captured gas quantity dropped from 0.029 mol to 0.021 mol. Similarly, as shown in Fig. 6(a), the CO_2 capture rate decreased from 63.1 % to 55.6 % with increasing temperature, as lower temperatures favor the formation of gas clathrate complexes. The separation factor increased with rising temperature, as higher temperatures prevent N_2 from entering the clathrate phase. As indicated in Fig. 6(b), the concentration of CO_2 in the gas phase rose from 6.2 mol% to 7.2 mol %. Enhanced clathrate formation driven by lower temperatures strengthens the clathrate formation tendency and improves the incorporation of CO_2 into the clathrate phase. According to both phase equilibrium and kinetic studies, a greater temperature-driven driving force was found to improve the efficiency of CO_2 capture. At the lowest experimental temperature of 280.6 K, the CO_2 capture rate reached a maximum of 63.1 %, with the CO_2 SF increasing from 55.0 to 203.9. As the temperature decreased, more N_2 entered the clathrate phase, capturing CO_2 and reducing the CO_2 concentration in the clathrate phase from 94.1 mol% to 81.4 mol%.

3.3. *Initial Gas-Liquid ratio on separation performance*

Both temperature and pressure analyzed above are key factors influencing the thermodynamic equilibrium of clathrates. Additionally, the initial R_v under operating conditions significantly impacts the clathrate separation process. Therefore, the effect of different initial gas-liquid volume ratios on clathrate separation efficiency was further investigated. Table S3 summarizes the results at different gas–liquid ratios. For flue gas, clathrate reaction experiments were conducted under a series of different R_v. Experimental conditions were set at a temperature of 280.6 K and an initial pressure of 3.0 MPa, with R_v ranging from 28.3 to 170.9.

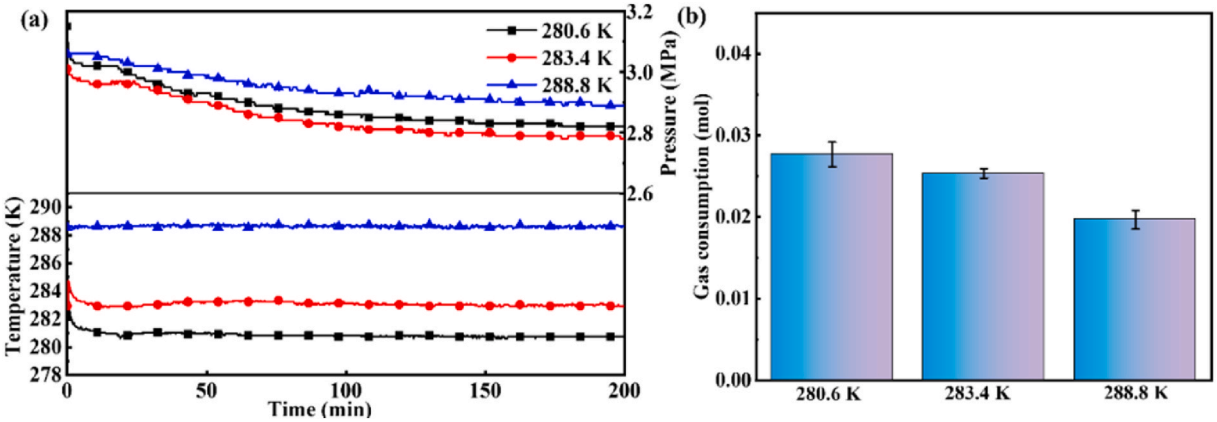

Fig. 5. (a) Pressure changes and (b)gas consumption during clathrate formation at different temperatures, 3.0 MPa, and in 72.0 wt % Gua_2SO_4 solution.

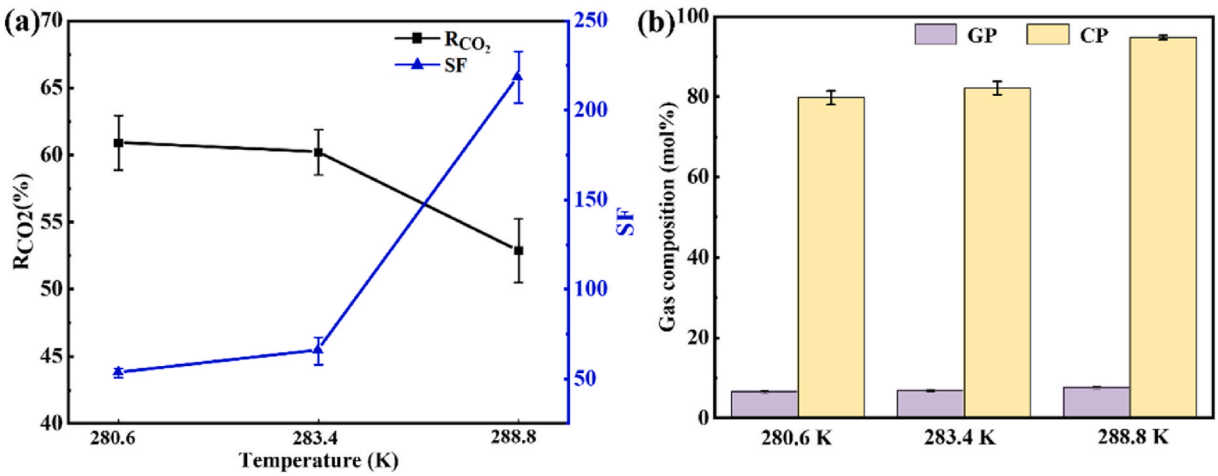

Fig. 6. (a) CO_2 capture rate and separation factor, (b) the CO_2 concentration in the gas phase and clathrate phase at different temperatures, 3.0 MPa, and in 72.0 wt % Gua_2SO_4 solution.

Fig. 7(a) displays three curves representing the pressure changes of the flue gas at different R_v. The blue curve corresponds to $R_v = 28.3$, the red curve to $R_v = 77.0$, and the green curve to $R_v = 170.9$. As shown in Fig. 7(a) and (b), the gas capture rate at initial $R_v = 77.0$ fell between that of $R_v = 170.9$ and $R_v = 28.3$. It decreased by approximately 0.1 MPa within about 0.25 h but subsequently declined at a slower rate than $R_v = 170.9$, stabilizing at 2.80 MPa with a total pressure drop of 0.21 MPa. A higher initial R_v value indicates a greater gas flow rate per unit volume of liquid. This provides a more abundant gas supply, resulting in significantly increased absolute gas consumption over time. As shown in Fig. 7(b), gas capture was maximized at the highest gas-to-liquid ratio. A higher gas-to-liquid ratio requires greater gas volume to achieve saturation in the solution. This ratio facilitates the formation of finer bubbles, promoting more uniform gas-liquid mixing and more gas clathrates are generated through the reaction.

At 3.0 MPa and 280.6 K, as shown in Fig. 8(a), the CO_2 capture rate and separation factor gradually decreased after the system reached hydration equilibrium as R_v increased from 28.3 to 170.9. As the R_v increased from 28.3 to 170.3, the CO_2 capture rate decreased from 79.5 % to 49.9 %, and the separation factor dropped from 80 to 14.6. At low R_v, sufficient liquid volume enables capture of more CO_2 gas. It is evident that reducing the R_v significantly enhances gas capture efficiency and separation performance.

As shown in Fig. 8(b), with increasing R_v, the CO_2 concentration in the gas phase rose from 4.4 mol% to 8.5 mol%. This increase resulted from the elevated R_v, where a reduced volume of reaction liquid was unable to capture more gas molecules. The CO_2 concentration in the clathrate increased from 76 % to 81.4 % before decreasing to 69.3 %. Increasing R_v expanded the gas-liquid interface area (more or smaller bubbles), providing greater opportunities for CO_2 dissolution. Raising the R_v significantly enhanced CO_2 mass transfer, thereby fully enabling selective capture effects and continuously increasing the CO_2 concentration in the clathrate phase, which in turn further increases the R_v. When water volume is limited and gas is in excess, the chance for N_2 molecules to "accidently" enter the clathrate phase rises significantly, which also contributes to the decrease in CO_2 concentration within the clathrate phase.

Whit high R_v (170.9), CO_2 capture rate was low, while low R_v (28.3) resulted in lower CO_2 concentration in the clathrate phase. A low R_v also implied an increased liquid volume, which raises agitation energy consumption and progressively reduced the volume of gas that can be processed. At a R_v of 77.0, CO_2 capture, and separation efficiency showed the most pronounced improvement, thus selecting R_v 77.0 as the reaction gas-liquid rate.

4. Process simulation analysis

4.1. Technological roadmap

Fig. 9 shows the ASPEN Plus simulation diagram for CO_2 capture from flue gas via clathrate promoted by Gua_2SO_4. The clathrate-based process for CO_2 capture primarily comprises key operational units for

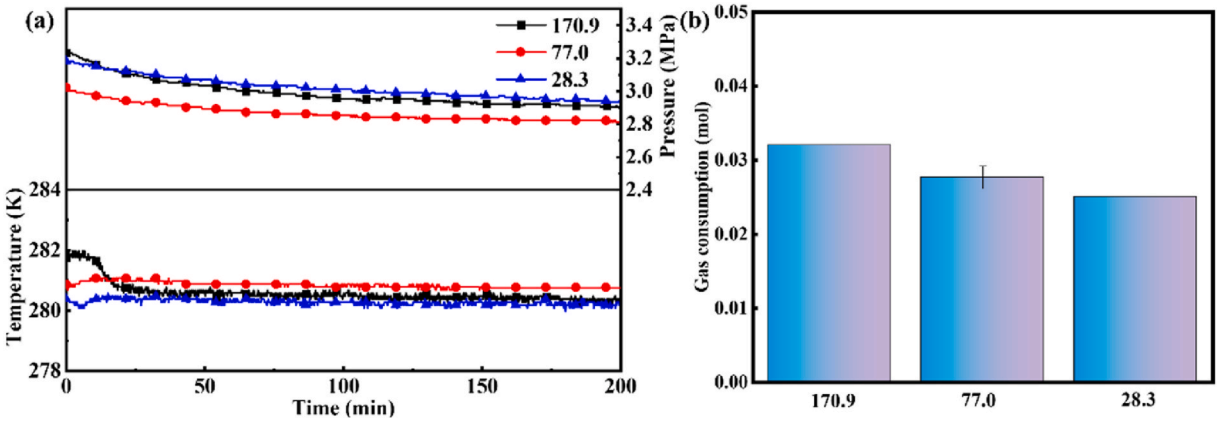

Fig. 7. (a)Pressure changes and (b)gas consumption during clathrate formation under conditions of different R_v, at 280.6 K, 3 MPa, and in 72.0 wt% Gua_2SO_4 solution.

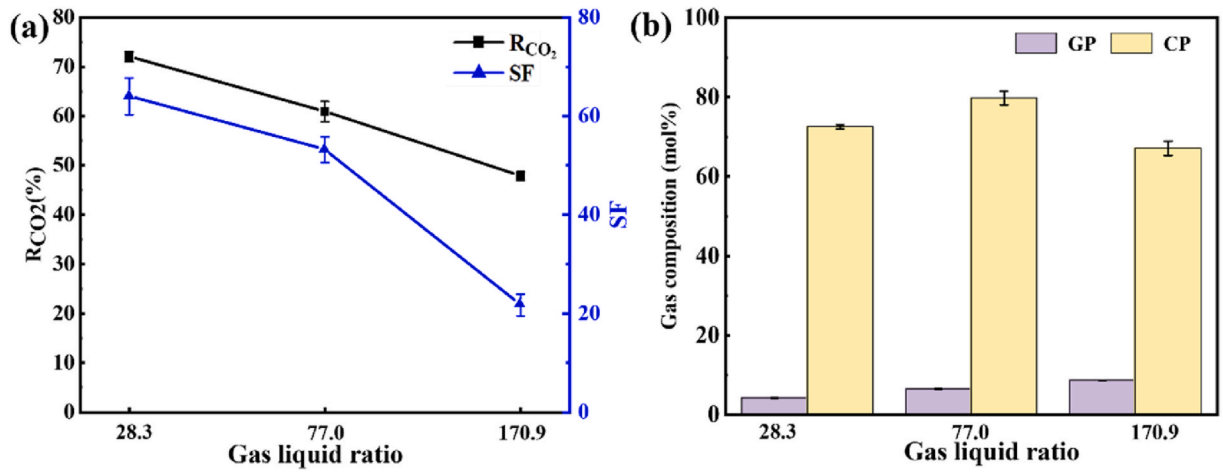

Fig. 8. (a) CO_2 capture rate and separation factor, (b) CO_2 gas phase and clathrate phase gas concentrations under conditions of different R_v, at 280.6 K, 3.0 MPa, and in 72.0 wt% Gua_2SO_4 solution.

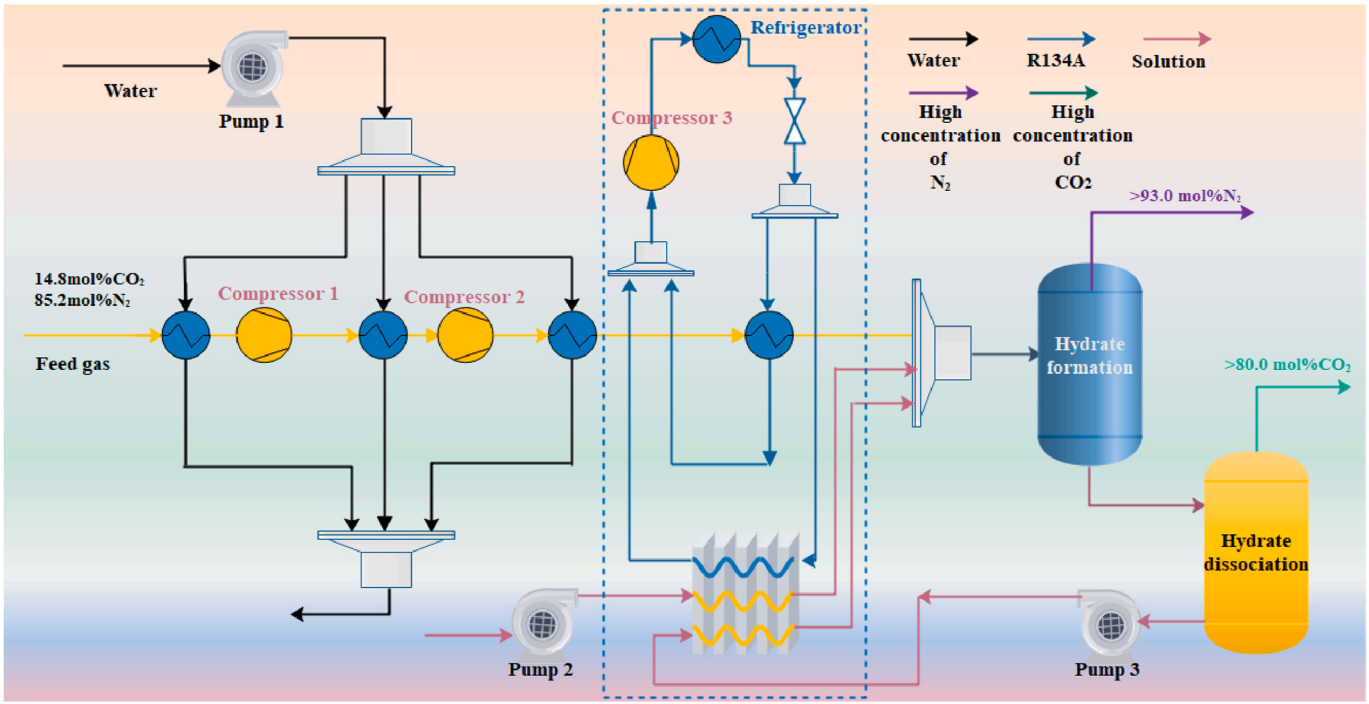

Fig. 9. Schematic diagram of clathrate -based carbon capture technology.

compression, refrigeration, and clathrate formation/dissociation, along with an integrated energy recovery system.

4.1.1. Clathrate separation process

Flue gas simulation data were sourced from Tajima et al. (2004), with a flow rate of 1074 t/h, initial temperature of 50 °C, and pressure of 0.1 MPa. The gas is pressurized to the target pressure and then cooled via a water-circulating cooler (Pump 1) to a temperature slightly above ambient. High-pressure conditions were required for clathrate formation, which is achieved by two compressors (Compressor 1 and Compressor 2). The feed gas pre-cooled passed through a secondary cooler to reach the precise temperature required for clathrate formation, thereby minimizing refrigeration energy requirements. It subsequently enters the stirred reactor under conditions optimal for clathrate nucleation and growth. Since the exothermic clathrate formation raised the reactor temperature, a low-temperature refrigerant, such as R134a, was used to maintain a constant reactor temperature. During clathrate formation, higher CO_2 concentrations facilitate the formation of clathrates. The CO_2-rich clathrate slurry enters the dissociation vessel, where it undergone heat exchange with ambient fluid and dissociated at atmospheric pressure. After dissociation, the clathrate re-enters the agitated reactor for clathrate formation. The reaction solution operated at ambient pressure and required pressurization via a fluid pump to meet clathrate formation conditions. The Gua_2SO_4 reaction solution circulates throughout the process. The clathrate formation/dissociation apparatus yielded N_2-rich and CO_2-rich gases. The CO_2-rich gas was discharged from the top of the clathrate dissociation apparatus. The dissociated water is repressurized using a fluid pump, cooled via a refrigeration cycle, and returned to the clathrate formation apparatus. Clathrate dissociation requires heating using ambient fluid at an air temperature and pressure of 298.2 K and 0.1 MPa.

4.1.2. Clathrate formation unit

In this simulation process, the formation and dissociation of clathrates are continuous, disregarding variations in clathrate formation rates caused by changes in driving forces. The driving force was therefore characterized as the deviation of the initial operating pressure from the equilibrium pressure at the corresponding temperature. Furthermore, the equilibrium clathrate formation conditions were governed by the initial molar composition of the gas mixture. Thus, the reaction driving force and undercooling were determined by the initial reaction conditions. A high-pressure, low-temperature gas mixture was introduced into a continuously stirred clathrate formation apparatus designed to reduce mass transfer resistance and enhance clathrate formation rates. Within this apparatus, the gas mixture reacted with the solution to form clathrates. The processes of clathrate formation and dissociation were modeled using the Chen-Guo two-step clathrate formation model and the Peng-Rob state equation.

The enthalpy of decomposition for CO_2 capture based on clathrates is calculated using the Clausius-Clapeyron equation, which can be described by equation (7), (Zhou et al., 2018).

$$\frac{d\ln P}{d(1/T)} = \frac{-\Delta H_{diss}}{ZR} \tag{7}$$

In equation (7), P and T represent the phase equilibrium pressure and temperature of the CO_2 clathrate, respectively; Z is the gas compression factor; R is the universal gas constant; and ΔH_{diss} the enthalpy of decomposition of the CO_2 clathrate.

The specific energy consumption for CO_2 capture was calculated as:

$$E_{spec} = \frac{W_{total}}{m_{CO_2}} \tag{8}$$

where W_{total} (kW) is the total power consumption of compressors, pumps, refrigeration units, and agitation, and m_{CO2} is the mass flow rate of captured CO_2 obtained from the process simulation. The resulting value was converted to kWh/kg CO_2 using a 1-h operating basis.

Highly concentrated electrolyte solutions can alter gas solubility and fugacity through strong ion–water interactions and activity effects, which may influence gas–liquid partitioning and thereby introduce a systematic deviation in uptake estimation if dissolution is non-negligible. Accordingly, the uptake values reported here should be interpreted as apparent uptake dominated by clathrate formation under the investigated conditions. A more rigorous treatment would require coupling gas-phase fugacity calculations with an electrolyte activity model to quantify gas dissolution and non-ideality in the liquid phase. Such modeling, together with targeted solubility measurements, will be pursued in future work to refine phase-behavior description and improve the accuracy of gas uptake evaluation.

4.2. Process parameters

4.2.1. Experimental parameters

The experimental data used in this study ensure the reliability of subsequent computational analyses. Detailed experimental values applied in the process simulations are summarized in Tables 1 and 2, while Table 3 lists the unit types employed along with their corresponding parameter specifications. As illustrated in Fig. 10, the slope necessary for applying the Clausius–Clapeyron equation was derived through linear regression performed using Origin software. The confidence intervals were derived from the standard errors of the linear regression. The intercept and slope were determined as 19.53 ± 0.97 and −5346.94 ± 278.13, respectively, yielding an average dissociation enthalpy of $\Delta H_{diss} = 44.45 \pm 2.31$ kJ mol^{-1}. Residual analysis (Fig. S1) shows that the residuals are randomly distributed around zero, indicating that the linear assumption is appropriate, and that no significant heteroscedasticity or nonlinearity exists within the investigated pressure range of 2.0–3.2 MPa. This supports the applicability of the Clausius–-Clapeyron approximation for the present system. Although independent measurements under identical conditions were not conducted, the employed methodology is consistent with that reported in the literature, supporting the validity of the present analysis (Huang et al., 2022).

Table 1
Specific experimental data from process simulation.

Pressure	Temperature	G/L	CO_2 capture/%	Reactor outlet pressure	Stirring time
2.0 MPa	280.6 K	81.2	51.5	1.85 MPa	60 min
3.0 MPa	280.6 K	77.1	63.1	2.80 MPa	60 min

Table 2
Compressibility factor and clathrate dissociation enthalpy under different pressure.

Pressure	Compressibility factor	ΔH_{diss}/(kJ/mol)
2.0 MPa	0.98315	44.03
2.3 MPa	0.98193	43.97
2.7 MPa	0.97987	43.88
3.0 MPa	0.97968	43.82
3.2 MPa	0.97771	43.79

Table 3
Unit types involved in process simulation and parameter specifications.

Block name	Type	Parameters and regulations
Comp 1 Comp 2 Comp 3	Compression	Polytropic efficiencies: 0.8[a]
Refrigerator	Refrigerator (Cooling medium: R134a)	Specified outlet temperature; Pressure drop, 0 MPa[a] COP = 2.24[b]
Pump 1 Pump 2 Pump 3	Pumping	Pump efficiencies: 0.8[a]; Driver efficiencies: 0.95[a]; Specified discharge pressure
Formation/ dissociation	Component splitter	Specified split fraction and outlet flash

[a] Since the clathrate-based flue gas capture CO_2 process has no actual pilot plant process data for reference, the adopted parameters are ideal. Meanwhile, the adopted data are also combined with the data used in similar work (Huang et al., 2022).

[b] COP = 2.24 calculated by Aspen HYSYS V12 (cooling medium: R134a) was obtained in a separate run considering only the refrigeration system.

4.2.2. Process assumptions

Under suitable temperature and pressure conditions for clathrate formation, nucleation does not occur instantaneously. At this initial stage, clathrate growth is hindered, and the actual formation temperature tends to be lower than the theoretical equilibrium value. This phenomenon is attributed to the requirement of a certain degree of undercooling-defined as the temperature depression below the phase equilibrium temperature under constant pressure. To promote immediate clathrate nucleation upon gas-liquid contact, an undercooling of 12.0 K is applied. Once a critical amount of clathrate has formed, its continued presence autocatalytically sustains further clathrate generation, thereby establishing the basis for a continuous separation process. In engineering contexts, equipment is generally insulated to minimize heat loss. For modeling simplicity, the present study assumes that heat exchange occurs only with dedicated cold and hot sources during clathrate formation and dissociation, and not with the ambient environment. This assumption supports the treatment of the overall process as continuous. Previous studies have identified gas-liquid mass transfer as the rate-limiting step in clathrate formation kinetics. The addition of a promoter Gua_2SO_4 improves the dissolution and mass transfer of gas molecules to the aqueous phase, significantly reducing the induction period without altering the system's thermodynamic conditions.

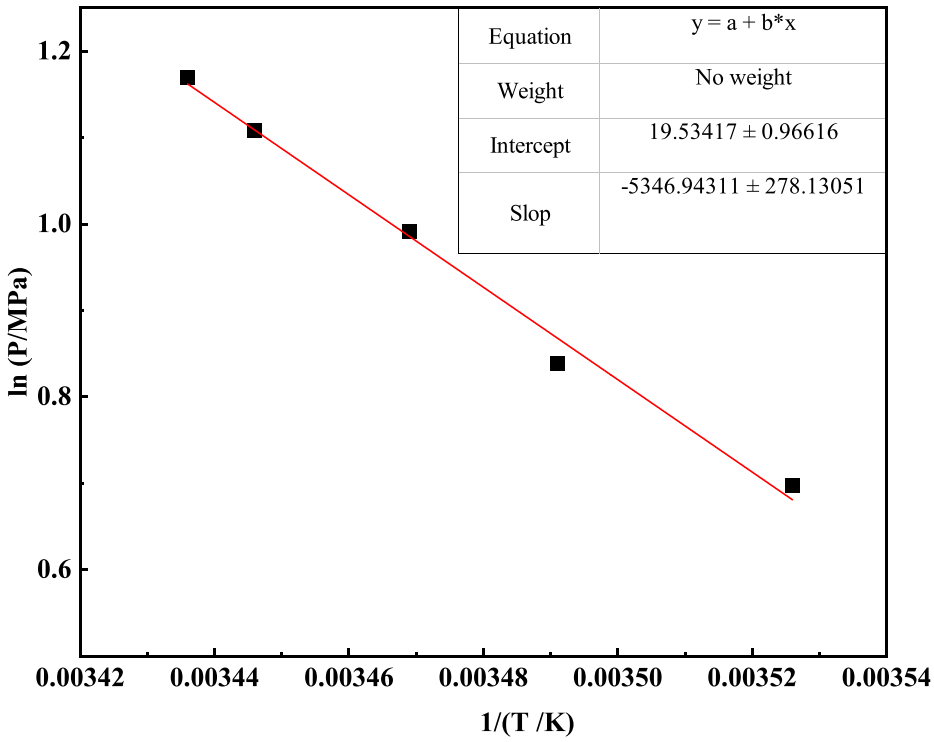

Fig. 10. Linear fitting of phase equilibrium data.

4.2.3. Energy consumption composition

All energy consumption values reported in this section were obtained from steady-state process simulations performed in Aspen Plus based on the experimental separation performance. The simulated flue gas feed rate was 1074 t h^{-1}, with an inlet temperature of 70 °C and pressure of 0.1 MPa. Key process streams were defined by their pressure, temperature, and mass flow rate, and the corresponding power requirements of compressors, pumps, agitators, and refrigeration units were directly calculated by the simulator using the specified equipment efficiencies listed in Table 3. These unit power consumptions were subsequently summed to obtain the total process power demand under each operating condition. The compressor power was calculated using polytropic compression with an assumed efficiency of 0.8, which is representative of industrial-scale centrifugal compressors. Multi-stage compression with intercooling was implicitly considered by specifying the outlet pressure and efficiency in Aspen Plus. The refrigeration duty was evaluated using a coefficient of performance (COP) of 2.24, corresponding to typical industrial refrigeration systems operating near the investigated pressure range (~280 K). Energy recovery through pressure expansion and cold-energy utilization was modeled by integrating expanders and heat exchangers with idealized recovery efficiencies, providing an upper-bound estimate of the achievable energy savings. Fig. 11(a) and (b) present the simulated energy consumption profiles for the compressor, pump, and clathrate reactor under the process conditions of 3.0 MPa and 280.6 K. The compressor was used to compress gas into the clathrate formation apparatus. Due to the high volumetric flow rate, compression required a substantial amount of energy. The compression energy consumption for the clathrate process was 121807.0 kW, accounting for 80.97 % of the total. The entire process required temperature reduction to maintain reaction progress, with the refrigeration module consuming 11323.0 kW of energy, representing 7.53 % of the total. Pumps consumed energy to transport fluids, totalling 96492.0 kW, accounting for 6.42 %. Agitation throughout the process consumed 7637.6 kW, which represents 5.08 % of the total energy consumption.

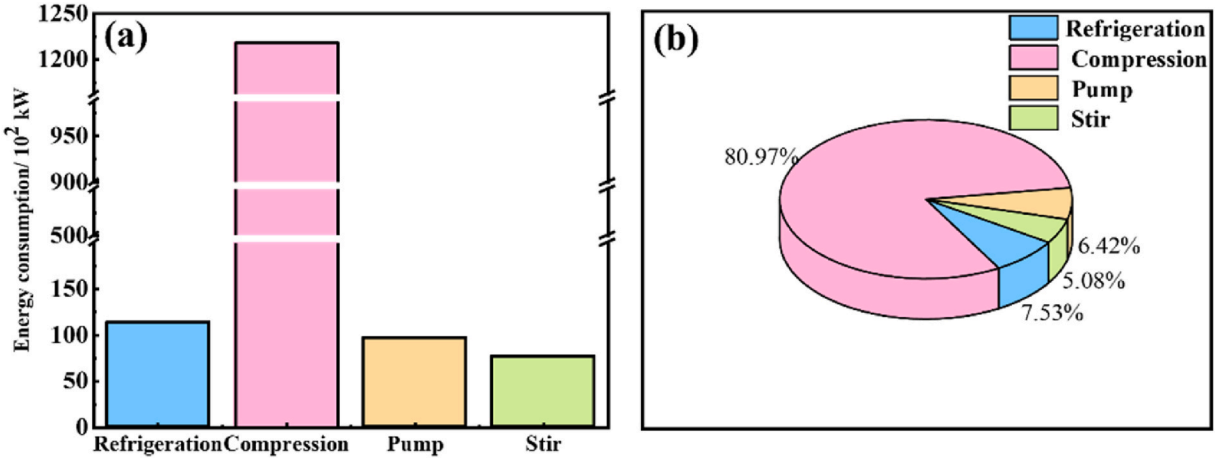

Fig. 11. (a)Energy consumption and (b)Proportion by module (3.0 MPa, 280.6 K).

The process captured 165396.0 kg/h of CO_2, with a capture energy consumption of 0.91 kWh/kg(The energy consumption was calculated using Equation (8).).

The implementation of energy optimization measures is pivotal for curtailing consumption, elevating energy efficiency, and diminishing operational expenditures. Energy recovery was implemented throughout the entire clathrate formation process. Enhanced recovery and utilization of pressure energy from separated gases are achieved by designing more advanced energy recovery equipment and process flows, thereby improving the overall energy utilization of the process system. The cold energy from the clathrate dissociation process was utilized for pre-cooling the feed gas prior to compression. The cold energy gas from N_2 and the target gas were used for further pre-cooling and compression of the feed gas. Finally, a refrigeration unit cooled the feed gas to meet the temperature requirements for clathrate formation. As shown in Fig. 12, cold energy and compression work are recovered from the target gas. A pressure energy recovery unit was integrated into the system to harness the high-pressure potential of the target gas following clathrate formation. The target gas passing through the turbine generates both pressure energy and cold energy. As shown in Fig. 13(a) and (b), the compression energy consumption of the recovered clathrate process was 73350.2 kW, accounting for 72.53 % of the total energy consumption. By utilizing the cold energy released during pressure reduction to cool the gas while recovering the compression work, the refrigeration energy consumption was reduced to 10503.0 kW, representing 10.38 % of the total energy consumption. Unit energy consumption for CO_2 capture: 0.69 kWh/kg.

Using the same calculation method, energy consumption calculations for the compressor, pump, and clathrate reactor were performed in the process simulation at 2.0 MPa and 280.6 K. As shown in Fig. 14(a) and (b), the compression energy consumption was 101357.0 kW, accounting for 80.42 % of the total power consumption; The refrigeration module consumed 98543.0 kW, accounting for 7.82 % of total power consumption; the pump consumed 55675.0 kW, representing 4.42 % of total power consumption; and the stirring process consumed 92510.0 kW, constituting 7.34 % of total power consumption. After reducing pressure from 3.0 MPa to 2.0 MPa, total energy consumption decreased by 24387.2 kW. The amount of captured CO_2 decreased from 165396 kg to 146960 kg, and the energy consumption per kg of captured CO_2 decreased from 0.91 to 0.85 kWh/kg.

The recovery of work and cooling energy from the exhaust gas, as shown in Fig. 15(a) and (b), resulted in a compression energy consumption of 59708.0 kW, accounting for 71.53 % of the total power consumption. The refrigeration module consumes 8946.7 kW (10.72 % of total power), the pump consumes 5567.5 kW (6.67 %), and the agitator consumes 9251.0 kW (7.34 %). The unit energy consumption for CO_2 capture was 0.56 kWh/kg CO_2. After pressure recovery, the formation pressure of the clathrate decreased from 3.0 MPa to 2.0 MPa, resulting in a 17.5 % reduction in overall process energy consumption. This demonstrates that lowering the pressure can significantly reduce process energy consumption. For the two representative operating pressures (2.0 and 3.0 MPa at 280.6 K, $R_v = 77.9$), the results show a clear trade-off between capture rate, selectivity, and energy demand. As summarized in Table 1, increasing the pressure to 3.0 MPa achieves a CO_2 capture rate of 63.1 %, maintaining high separation performance. The CO_2 concentration in the clathrate phase remains high (83.9 mol% at 2.0 MPa vs. 81.4 mol% at 3.0 MPa), and the CO_2/N_2 separation factor shows only a minor change across the two pressures. However, the benefit of pressurization must be weighed against the higher specific energy consumption, which increases from 0.56 kWh·kg^{-1} CO_2 at 2.0 MPa to 0.69 kWh·kg^{-1} CO_2 at 3.0 MPa. It should be noted that the lowest specific energy consumption value of 0.56 kWh·kg^{-1} CO_2, obtained at 2.0 MPa with pressure and cold-energy recovery, represents an optimistic lower-bound scenario based on thermodynamic equilibrium simulation. While reducing the operating pressure significantly decreases compression work and overall energy demand, it also leads to a noticeable reduction in CO_2 capture rate (from 63.1 % at 3.0 MPa to 51.5 % at 2.0 MPa, Table 1) and a corresponding decrease in the absolute amount of CO_2 captured per unit time. From a process perspective, this implies a trade-off between minimizing specific energy consumption and maintaining sufficient capture throughput. Therefore, the optimal operating pressure should be determined by jointly considering energy efficiency, CO_2 recovery, and processing capacity, rather than targeting the minimum energy consumption alone. As shown in Fig. 16,

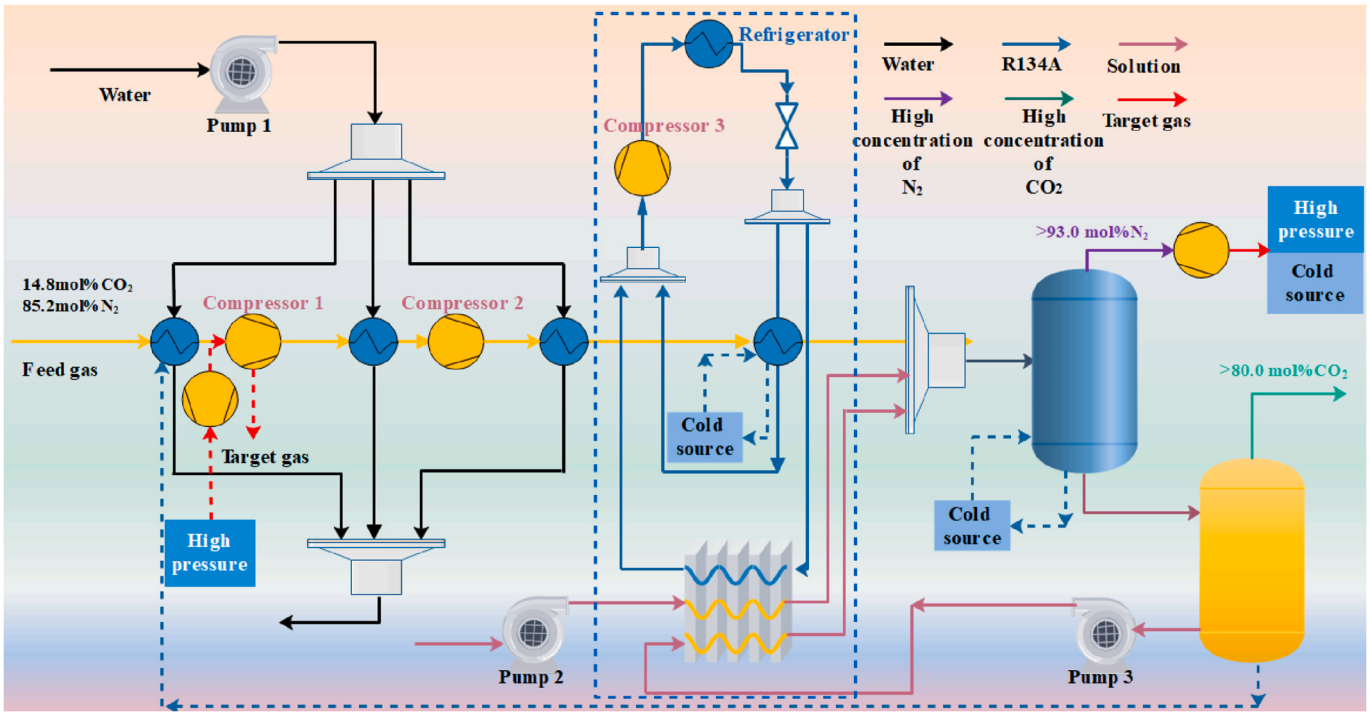

Fig. 12. Specific flowchart of the process after energy optimization.

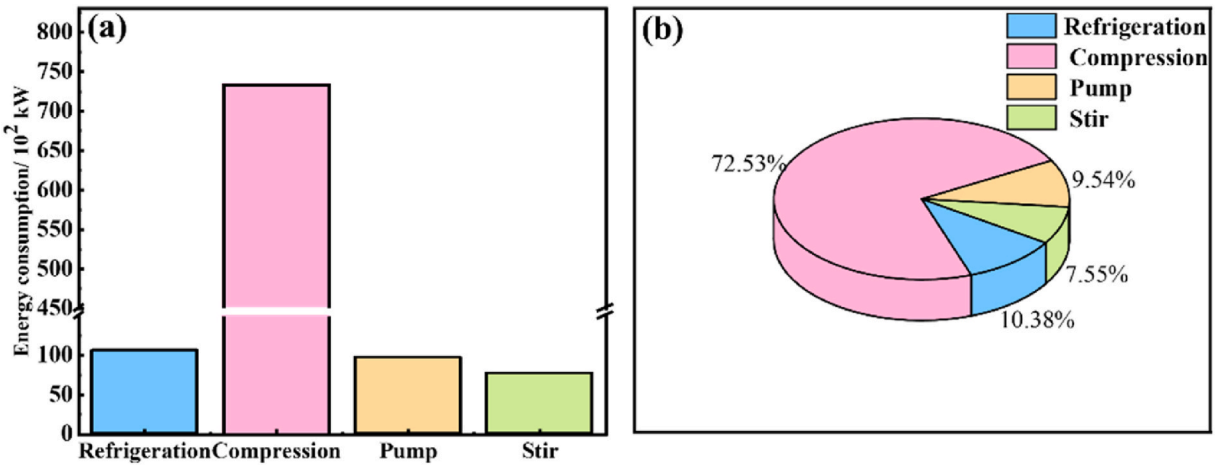

Fig. 13. (a)Energy consumption and (b)proportion of each module after compression work recovery.

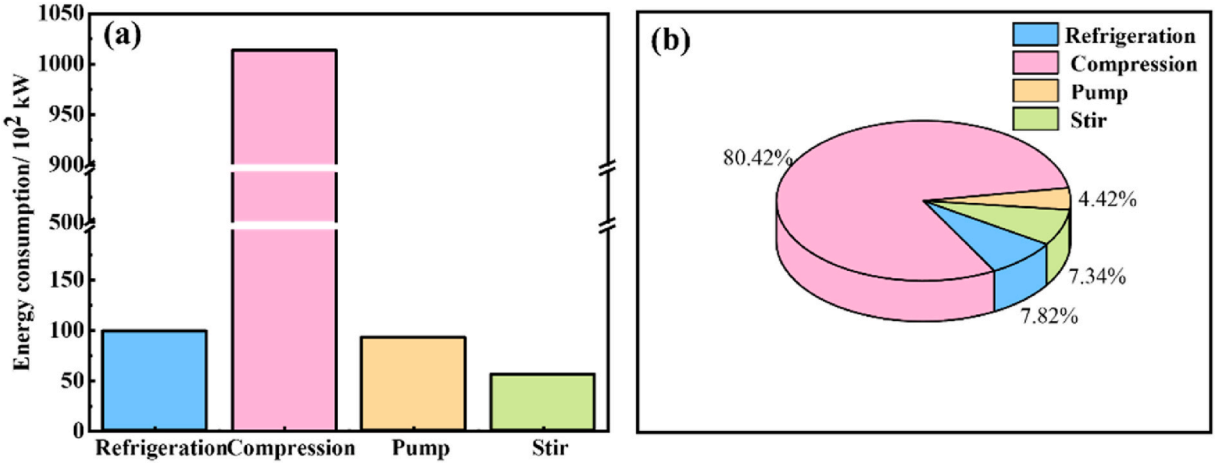

Fig. 14. (a)Energy consumption and (b)proportion by module (2.0 MPa, 280.8 K).

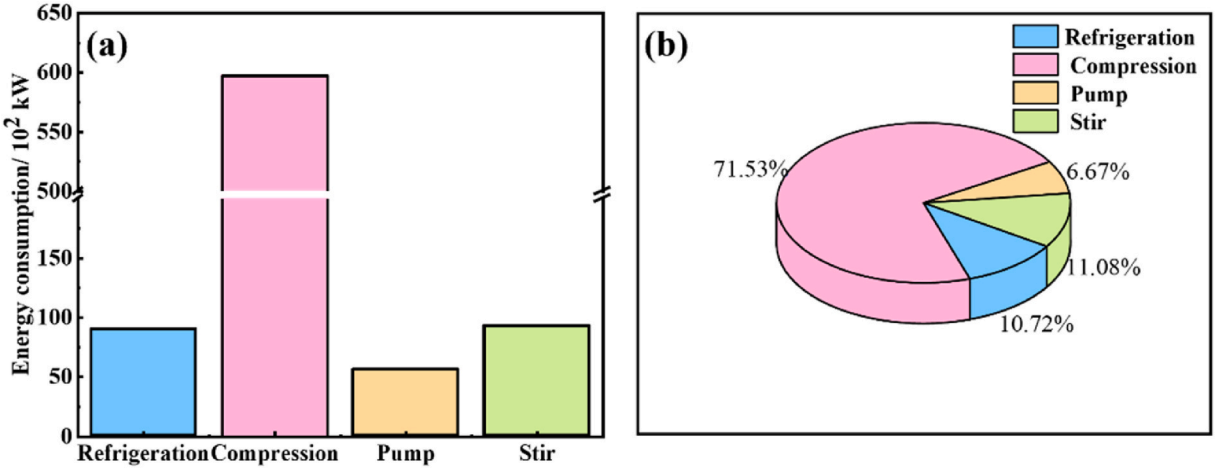

Fig. 15. (a)Energy consumption and (b)proportion of each module after compression work recovery.

experimental results and calculations were compared with data from the literature, showing that this study achieves relatively low energy consumption for CO_2 capture. In this work, the energy consumption is reported as specific electrical energy per unit CO_2 captured ($kWh \cdot kg^{-1}$ CO_2) under the corresponding experimental separation performance (capture rate and outlet phase compositions). This metric allows a first-order assessment of process potential; however, it does not fully eliminate differences in boundary conditions relative to mature technologies. For example, absorption-based capture is often evaluated at near-atmospheric pressure but includes thermal regeneration duty, whereas the clathrate process requires gas pressurization (2-3 MPa) and refrigeration, and its net advantage depends on balancing selectivity/product

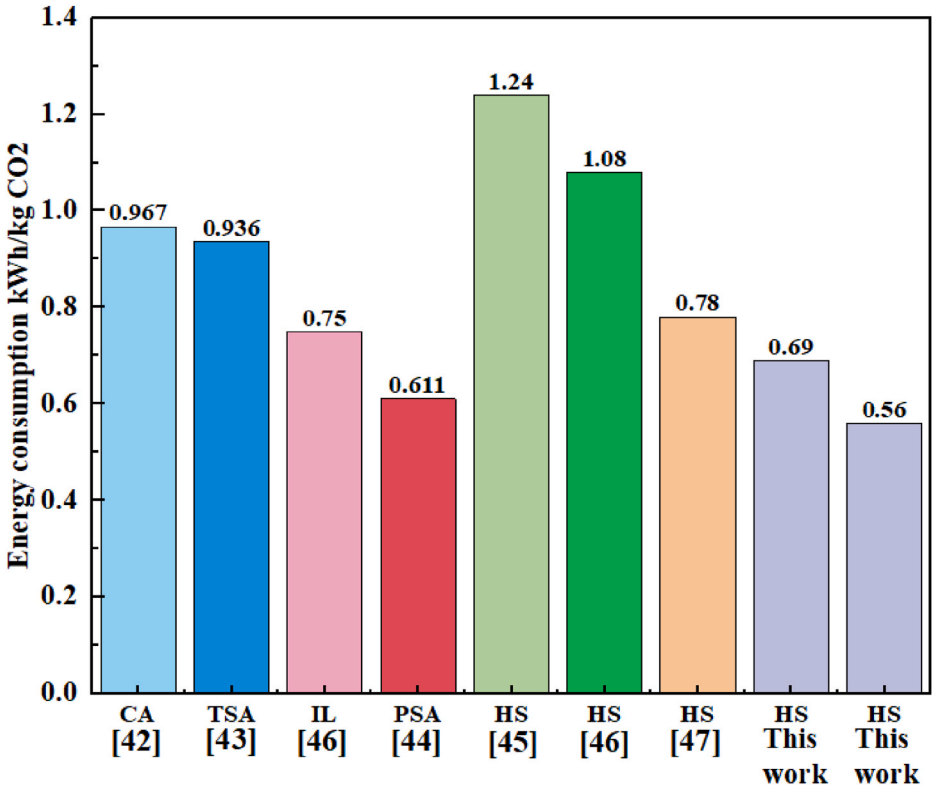

Fig. 16. Comparison of energy cost for different flue gas separation technologies (Lungkadee et al., 2021; Ntiamoah et al., 2016; Ribeiro et al., 2017; Xie et al., 2019; Feyzi and Mohebbi, 2020; Xiao et al., 2024). *CA-Chemical Absorption, TSA- Temperature Swing Adsorption, IL- Ionic Liquid separation, PSA- Pressure Swing Adsorption, HS-Hydrate separation.

purity against compression penalties. Accordingly, the term "low energy consumption" in this study should be interpreted as promising within the investigated operating window and under the stated assumptions, rather than as a direct one-to-one superiority claim over commercial capture processes. A rigorous benchmarking study—normalizing feed specifications, capture targets, and process boundaries—will be pursued in future work to enable an equal-basis comparison with mature CO_2 capture technologies. It is important to note that the energy consumption values reported herein are based on thermodynamic equilibrium simulations and represent the theoretical minimum requirement. The actual energy demand in a commercial plant is expected to be higher due to practical limitations not captured in the model, such as kinetic barriers to clathrate formation, heat losses in the process equipment, non-ideal heat exchanger performance, and pressure drops across the system. Future work will focus on experimental validation of these energy requirements under dynamic operating conditions.

Although the Gua_2SO_4-promoted clathrate process operates at significantly lower pressures than clathrate formation in pure water, the required pressure range (2-3 MPa) is still higher than that of widely deployed absorption-based post-combustion capture systems. Consequently, the compression work and associated capital/operating costs are expected to be non-negligible and must be considered when evaluating the industrial feasibility of the process. In practice, the overall attractiveness of the process depends on whether the benefits of high CO_2 enrichment/selectivity and simultaneous N_2 recovery outweigh the energy and integration costs associated with pressurizing a large-volume flue-gas stream. From an integration perspective, compression-related penalties can be mitigated through multistage compression with intercooling, which reduces compression work and enables recovery of low-grade heat. Although the present analysis indicates favorable specific energy consumption under the investigated conditions, future work should include plant-level integration and economic assessments—covering compressor design, heat integration, and flue gas pretreatment—to fully evaluate the cost implications of operation at 2-3 MPa.

While the Gua_2SO_4-based clathrate process demonstrates promising separation performance, it is important to recognize that guanidinium salts should not be assumed to be environmentally benign in the event of an accidental release. As such, any practical deployment of this technology must include rigorous environmental, health, and safety controls. From a process intensification perspective, the promoter solution should ideally be managed in a closed-loop configuration, where the concentrated Gua_2SO_4 solution is efficiently recovered and recycled to minimize make-up requirements and reduce the potential for discharge. Regarding handling and spill mitigation, standard engineering safeguards are recommended, including the selection of corrosion-resistant materials for wetted parts, sealed storage and transfer systems, and secondary containment structures to prevent soil and groundwater contamination. In the event of a release, spill-response measures should prioritize rapid containment, collection, and controlled clean-up. In this study, all experiments under a given set of conditions were conducted using the same batch of Gua_2SO_4 solution, and no noticeable degradation or loss of separation performance was observed across repeated formation–dissociation cycles at the laboratory scale. In addition, previous studies have demonstrated that Gua_2SO_4-based clathrate systems can undergo multiple cycles without significant promoter degradation or performance loss, owing to the high chemical and thermal stability of Gua_2SO_4. Nevertheless, systematic long-term cyclic testing and quantitative assessment of promoter loss and recovery efficiency will be essential in future work to support scale-up and industrial implementation (Xiang et al., 2023).

Water management is an important practical factor for clathrate-based CO_2 capture processes, particularly when a highly concentrated promoter solution is used. During clathrate dissociation and phase handling, changes in liquid holdup, water carryover with gas streams, and condensation/evaporation effects may lead to gradual dilution of

the Gua_2SO_4 solution. In addition, repeated cycling may introduce minor water accumulation (or loss) depending on the configuration of gas cooling, separation, and recycle streams. Because promoter concentration directly affects clathrate separation performance, dilution may increase make-up requirements and affect long-term operability and cost. Practical applications therefore require closed-loop liquid management and concentration control. While the present study reports performance at fixed laboratory compositions, future work will address concentration drift, make-up demand, and their impacts on capture performance, energy consumption, and overall process feasibility through quantitative water balance and multicycle operation.

It is worth noting that, at the operating temperatures explored in this work (around 280 K), the 72 wt% Gua_2SO_4 solution could be handled and mechanically stirred in the 250 mL reactor without operational difficulty, enabling stable and reproducible measurements of pressure evolution and gas composition during clathrate formation. The need for systematic measurements of viscosity (0.23 Pa s), density (1.33 g/cm^3), and heat capacity (2.61 J/g K), as well as corrosion and long-term stability assessments, is clearly identified as an important direction for future work to support process scale-up and industrial implementation. However, this laboratory-scale operability does not directly guarantee industrial practicality, as scale-up will involve different hydrodynamics, slurry behavior, and heat/mass transfer limitations. Accordingly, future work will (1) quantify key thermophysical properties (viscosity, density, and heat capacity) over relevant pressure ranges, (2) evaluate the resulting pumping and mixing energy requirements, (3) conduct corrosion/compatibility screening for candidate construction materials, (4) assess recyclability and long-term stability over multiple cycles to support process design and scale-up, and (5) focus on quantifying promoter loss during operation and optimizing recovery strategies to ensure the process's sustainability and compliance with industrial discharge regulations.

5. Conclusions

A highly selective method for capturing CO_2 has been proposed. The effects of temperature, pressure, and gas-liquid ratio on gas capture performance, along with system pressure on energy consumption, were investigated. The specific conclusions and outlook are set out below:

(1) Compared to TBAB and TBAF, Gua_2SO_4 promoted CO_2 clathrate complex formation under milder conditions (higher temperature and lower pressure).
(2) Experimental results using a 72.0 wt% Gua_2SO_4 solution at 280.6 K and pressures of 2.0/3.0 MPa (R_v = 77.9) confirmed high process selectivity, achieving CO_2 concentrations of 83.9/81.4 mol% in the clathrate phase and increasing N_2 purity in the gas phase to 92.1/93.8 mol%.
(3) The process's techno-economic potential was further confirmed by energy consumption analysis, where optimized energy consumption values reached 0.69 kWh/kg CO_2 at 3.0 MPa and 0.56 kWh/kg CO_2 at 2.0 MPa.

The method thus allows simultaneous efficient CO_2 enrichment and N_2 recovery, presenting a promising strategy for flue gas separation. Although the present study demonstrates encouraging selectivity and low energy consumption, the experiments were limited to laboratory-scale conditions. Future work will further examine clathrate formation kinetics and assess the recyclability and long-term stability of the Gua_2SO_4 solution over multiple cycles. In addition, efforts will be devoted to developing and scaling up continuous operation and to investigating process integration to better evaluate industrial applicability.

CRediT authorship contribution statement

Chongwei Wang: Writing – original draft, Investigation. **Shuanshi Fan:** Writing – review & editing, Supervision, Project administration, Funding acquisition, Conceptualization. **Yanhong Wang:** Writing – original draft, Visualization, Resources, Project administration. **Xuemei Lang:** Writing – original draft, Validation, Formal analysis. **Siyuan Chen:** Writing – original draft, Validation, Investigation. **Gang Li:** Validation, Software.

Notes

The authors declare no competing financial interest.

Declaration of competing interest

We declare that we have no known competing financial interests or personal relationships that could have appeared to influence the work reported in this paper.

Acknowledgement

This work was supported by the National Natural Science Foundation of China (NSFC, no. U25A20275).

Appendix A. Supplementary data

Supplementary data to this article can be found online at https://doi.org/10.1016/j.jgsce.2026.205900.

Data availability

Data will be made available on request.

References

Aghel, B., Janati, S., Wongwises, S., et al., 2022. Review on CO_2 capture by blended amine solutions. Int. J. Greenh. Gas Control 119, 103715.
Bai, J., Qiu, C., Wang, Y., et al., 2025. Separation of CO_2 from simulated flue gas by hydrate method in an impinging stream reactor. J. Environ. Chem. Eng. 13 (5), 118325.
Chen, S., Wang, Y., Lang, X., et al., 2023a. Rapid and high hydrogen storage in epoxycyclopentane hydrate at moderate pressure. Energy 268, 126638.
Chen, S., Wang, Y., Lang, X., et al., 2023b. Phase equilibrium of hydrogen clathrate hydrates with propylene oxide and 1,2-Epoxycyclopentane. J. Chem. Eng. Data 68 (5), 1184–1190.
Chen, S., Wang, Y., Fan, S., et al., 2024. Intriguing phenomenon of hydrogen molecules occupancy in clathrate hydrate cages: implications for hydrogen storage. Chem. Eng. J. 499, 156089.
Chen, W., Ye, F., Fan, S., et al., 2025. Corrigendum to manipulating pore structures of Ssz-13 zeolite membranes via hydrocracking activation for superior H_2/CO_2 separation. Microporous Mesoporous Mater. 388, 113551.
Davoodi, S., Al-Shargabi, M., Wood, D.A., et al., 2023. Review of technological progress in carbon dioxide capture, storage, and utilization. Gas Sci. Eng. 117, 205070.
Di Profio, P., Canale, V., D'Alessandro, N., et al., 2017. Separation of CO_2 and CH_4 from biogas by formation of clathrate hydrates: importance of the driving force and kinetic promoters. ACS Sustain. Chem. Eng. 5 (2), 1990–1997.
Eder, E., Kadinger, M., Hiller, S., et al., 2025. Hydrate-based carbon capture via pressure swing in a packed bed of ice. Sep. Purif. Technol. 361.
Englezos, P., Kalogerakis, N., Dholabhai, P.D., et al., 1987. Kinetics of formation of methane and ethane gas hydrates. Chem. Eng. Sci. 42 (11), 2647–2658.
Fan, S., Guo, T., 1999. Hydrate formation of CO_2-Rich binary and Quaternary gas mixtures in aqueous sodium chloride solutions. J. Chem. Eng. Data 44 (4), 829–832.
Fan, S., Li, S., Wang, J., et al., 2009. Effcient capture of CO_2 from simulated flue gas by formation oftbab or TBAF semiclathrate hydrates. Energy Fuel. (23), 4202–4208.
Fan, S., Long, X., Lang, X., et al., 2016. CO_2 capture from CH_4/CO_2 mixture gas with Tetra-N-Butylammonium bromide semi-clathrate hydrate through a pressure recovery method. Energy Fuel. 30 (10), 8529–8534.
Fan, S., You, S., Wang, Y., et al., 2019. Hydrate phase equilibrium of CH_4-Rich binary and ternary gas mixtures in the presence of Tetra-N-Butyl ammonium bromide. J. Chem. Eng. Data 64 (12), 5929–5934.
Feyzi, V., Mohebbi, V., 2020. Hybrid hydrate-membrane post-combustion CO_2 capture: a conceptual process design and analyses. Ind. Eng. Chem. Res. 59 (29), 13132–13142.
Fu, L., Ren, Z., Si, W., et al., 2022. Research progress on CO_2 capture and utilization technology. J. CO2 Util. 66, 102260.

Gao, N., Mao, X., Nan, N., et al., 2025. Hybrid Membrane/absorption-adsorption separation of hydrogen-blended natural gas at receiving terminal: process modelling and multi-objective optimization. Sep. Purif. Technol. 360, 131088.
Huang, H., Fan, S., Wang, Y., et al., 2022. Energy and exergy efficiency analysis for biogas De-CO_2 with Tetra-N-Butylammonium bromide hydrates. Energy 265, 126365.
Ito, H., Gibo, A., Shiraishi, S., et al., 2023. Renewed measurements of carbon dioxide hydrate phase equilibrium. Int. J. Thermophys. 44 (128), 1–15.
Lee, S., Lee, Y., Park, S., et al., 2010. Phase equilibria of semiclathrate hydrate for nitrogen in the presence of Tetra-N-Butylammonium bromide and fluoride. J. Chem. Eng. Data 55 (12), 5883–5886.
Lee, S., Park, S., Lee, Y., et al., 2011. Guest gas enclathration in semiclathrates of Tetra-N-Butylammonium bromide: stability condition and spectroscopic analysis. Langmuir 27 (17), 10597.
Lee, S., Lee, Y., Park, S., et al., 2012. Thermodynamic and spectroscopic identification of guest gas enclathration in the double Tetra-N-Butylammonium fluoride semiclathrates. J. Phys. Chem. B 116 (30), 9075–9081.
Li, X., Zhan, H., Xu, C., et al., 2012. Effects of Tetrabutyl-(Ammonium/Phosphonium) salts on clathrate hydrate capture of CO_2 from simulated flue gas. Energy Fuel. 26 (4), 2518–2527.
Li, Z., Zhong, D., Lu, Y., et al., 2016. Enhanced separation of carbon dioxide from a CO_2 + CH_4 gas mixture using a hybrid adsorption-hydrate formation process in the presence of coal particles. J. Nat. Gas Sci. Eng. 35, 1472–1479.
Li, G., Fan, S., Zhang, Z., et al., 2023. Mild ultraviolet detemplation of Sapo-34 zeolite membranes toward pore structure control and highly selective gas separation. Sep. Purif. Technol. 318, 123988.
Li, Z., Mu, X., Wei, W., et al., 2026a. A dual-functional ionic liquid biphasic absorbent for efficient CO_2 capture: enhanced capacity and reduced regeneration energy. Sep. Purif. Technol. 389, 136927.
Li, P., Yang, P., Jiang, B., et al., 2026b. Multi-objective optimization and performance analysis of a novel integrated system combined coal-fired power plant with compressed air energy storage and carbon capture. J. Energy Storage 151, 131206.
Lin, Y., Kong, C., Zhang, Q., et al., 2017. Metal-organic frameworks for carbon dioxide capture and methane storage. Adv. Energy Mater. 1601296 (7), 1–29.
Lungkadee, T., Onsree, T., Tangparitkul, S., et al., 2021. Technical and economic analysis of retrofitting a post-combustion carbon capture system in a Thai coal-fired power plant. Energy Rep. 7, 308–313.
Lv, Q., Zhang, K., Li, X., et al., 2023. Investigation on the structure, formation mechanism, and surface morphology of CP–CH_4 binary hydrate. Energy Fuel. 37 (3), 2009–2018.
Mohammadi, A.H., Richon, D., 2010. Ice clathrate hydrate gas phase equilibria for air, oxygen, nitrogen, carbon monoxide, methane, or ethane + water system. Ind. Eng. Chem. Res. 49 (8), 3976–3979.
Ntiamoah, A., Ling, J., Xiao, P., et al., 2016. CO_2 capture by temperature swing adsorption: use of hot CO_2-Rich gas for regeneration. Ind. Eng. Chem. Res. 55 (3), 703–713.
Peng, D., Robinson, D.B., 1976. A new two-constant equation of state. Ind. Eng. Chem. Fundam. 15 (1), 59–64.
Qi, J., Wang, Y., Fan, S., et al., 2018. Hydrate equilibrium measurements for CH_4 and CO_2/CH_4 mixture in the presence of single 2-Methyl-2-Propanol and 1,1-Dichloro-1-Fluoroethane. J. Chem. Eng. Data 63 (8), 3145–3149.
Ribeiro, A., Gleichmann, K., Ferreira, A.F.P., et al., 2017. Separation of CO_2/N_2 on binderless 5a zeolite. J. CO2 Util. 20, 224–233.
Seo, D., Lee, S., Lee, Y., et al., 2023a. Tailoring gas hydrate lattice dimensions for enhanced methane selectivity in biogas upgrading. Chem. Eng. J. 472, 145079.
Seo, D., Lee, S., Moon, S., et al., 2023b. Investigating two synthetic routes for gas hydrate formation to control the trapping of methane from natural gas. Chem. Eng. J. 467, 143512.
Sun, Q., Guo, X., Liu, A., et al., 2011. Experimental study on the separation of CH_4 and N_2 via hydrate formation in TBAB solution. Ind. Eng. Chem. Res. 50 (4), 2284–2288.
Tajima, H., Yamasaki, A., Kiyono, F., 2004. Energy consumption estimation for greenhouse gas separation processes by clathrate hydrate formation. Energy 29 (11), 1713–1729.
Wang, C., Fan, S., Wang, Y., et al., 2025. High purity carbon dioxide captured with guanidinium sulfate clathrate from carbon dioxide/hydrogen mixtures. Fluid Phase Equilib. 592, 114336.
Wang, F., Sengupta, B., Li, D., et al., 2026. Scalable nanoconfined ionic liquid membranes withultrapermeance and ultraselectivity for efficient CO_2 capture. Sci. Adv. 2 (12), 1329.
Wu, J., Zhang, Y., Yu, M., et al., 2025. High-efficient boil-off gas storage using low-temperature activated carbon adsorption. Gas Sci. Eng. 144, 205765.
Xia, Z., Zhao, Q., Chen, Z., 2022. Review of methods and applications for promoting gas hydrate formation process. Journal of natural gas science 101, 104528.
Xia, C., Liu, S., Yin, Q., et al., 2026. Ionic liquid-modified hollow microspheres of tartaric acid-anion intercalated ldh in Pim-1 membranes for superior CO_2/N_2 separation. J. Environ. Chem. Eng. 14 (2), 121277.
Xiang, Z., Liu, C., Chen, C., et al., 2023. Synthesis of stable single-crystalline carbon dioxide clathrate powder by pressure swing crystallization. Cell Rep. Phys. Sci. 4 (5), 101383.
Xiao, Y., Li, A., Li, B., et al., 2024. Energy consumption and economic analysis of CO_2 capture from flue gas by membrane separation coupled with hydrate method. Energy 312, 133471.
Xie, N., Liu, Z., Yang, S., et al., 2019. Energy efficiency analysis of postcombustion hydrate-based CO_2 capture with tetrahydrofuran and Tetra-N-Butylammonium bromide. Ind. Eng. Chem. Res. 59 (2), 802–813.
Xu, H., Xing, X., Chen, S., et al., 2025. Enhanced CO_2 capture from flue gas using tbaf semi-clathrate hydrates: a comprehensive thermodynamic and kinetic study. Chem. Eng. J. 508, 160955.
Yang, M., Zhou, H., Wang, P., et al., 2018. Effects of additives on continuous hydrate-based flue gas separation. Appl. Energy 221, 374–385.
Ye, F., Fan, S., Lang, X., 2024. Organic template residues confined in Silicalite-1 zeolite membranes for tuning pore structures and boosting H_2/CO_2 separation. Sep. Purif. Technol. 346, 127362.
Zhang, Y., Chen, F., Yu, S., et al., 2020. Biopromoters for gas hydrate formation: a mini review of current status. Front. Chem. 8, 1–6.
Zheng, J., Zhang, Y., Zhao, L., et al., 2024. A hydrate-based post-combustion capture system integrated with cold energy: thermodynamic analysis, process modeling and energy optimization. Energy Convers. Manag. 314, 118656.
Zhou, X., Long, Z., Tang, C., et al., 2018. Kinetic measurements on CO_2 hydrate formation in the presence of Tetra-N-Butyl ammonium bromide. Energy Fuel. 32 (9), 9683–9691.